physica status solidi b
www.pss-b.com

Check for updates

Characteristics of Ultrathin Indium Oxide Thin-Film Transistors with Diverse Channel Lengths Fabricated by Atomic Layer Deposition

*Ju-Hun Lee, Seung-Youl Kang, Jong-Heon Yang, Jae-Eun Pi, Chi-Sun Hwang, and Jaehyun Moon**

The oxide thin-film transistors (TFTs) with ultrathin (5 nm) crystalline In_2O_3 channels formed by an atomic layer deposition method are fabricated. The ultrathin In_2O_3 films are formed at a deposition temperature of 300 °C using (3-(dimethylamino)propyl)dimethylindium as the indium precursor and ozone as the oxidizing agent. The postannealing is performed in an oxygen atmosphere for 2 h at 300 °C. The scaling behavior of the field-effect mobility (μ_{FE}) is investigated as a function of the channel length (L_{ch}). As L_{ch} increases from 5 to 160 μm, the average μ_{FE} is measured and found to increase from 20.2 to 33.6 $cm^2\,V^{-1}\,s^{-1}$. It shows the average device properties of subthreshold swing of 0.32 V dec^{-1}, turn-on voltage of −5.5 V, and on/off current ratio of 107. To understand this trend, the transmission line model is utilized to extract the resistance components present across the channel quantitatively. The analyses reveal that among the components comprising the total resistance, the fraction of R_c increases as L_{ch} becomes shorter. Thus, R_c emerges as a dominant parameter that determines μ_{FE}. In this regard, the results have technical significance in vertical TFTs and high-resolution applications in which predictable scaling matters.

1. Introduction

The advent of amorphous oxide semiconductors has become a game changer for the backplane industry in place of amorphous silicon (a-Si:H).[1–6] This means these semiconductors meet the technical specifications for the next generation of display back-plane technology. Specifically, indium oxide (In_2O_3) is highlighted as a promising channel material due to its high mobility, optical transparency, compositional simplicity, low thermal budget, and other advantages.[7–9] It is optically transparent given its wide bandgap (≈3.7 eV)[10] due to the low energy of the oxygen 2*p* orbital that constitutes the upper part of the valence band.[11] In addition, because the spatially spread metal ns-orbitals (e.g., In 5*s*) with an isotropic shape are characterized by strong ionicity and direct overlap among themselves, they have high mobility, unlike hydrogenated amorphous silicon.[3,8,12–14] In particular, In_2O_3 film has an asymmetric band structure in which the fermi level (E_F) and the conduction band minimum (CBM) are close to 3.0 eV. Specifically, the thick In_2O_3 is considered to be a high conducting oxide due to the charge neutrality level (CNL) lying above 0.4 eV.[9,15,16] The weak binding energy of indium to oxygen tends to induce a state of oxygen deficiency.[17–19] These oxygen vacancies act as shallow donors in the oxide semiconductor, turning on the threshold voltage (V_{th}) at a negative voltage, and the higher the oxygen vacancy concentration, the higher the conductivity.[20] Previous studies have realized the stability and high mobility of ultrathin In_2O_3 thin-film transistors (TFTs) by controlling the film thickness and oxygen concentration with atomic layer deposition (ALD) and an oxygen annealing atmosphere, respectively. Lee[21] and Yeom[22] groups reported corresponding field-effect mobility outcomes of 41.2 and 39.2 $cm^2\,V^{-1}\,s^{-1}$. ALD techniques are attractive enough to be adopted as next-generation deposition methods owing to their self-limiting mechanism, in which the surface reactions stop and self-saturate when the surface-reactive are entirely depleted, enabling precise thickness and uniformity. In particular, compared to physical vapor deposition, ALD has superior deposition properties for miniaturized device processes.[23,24] Given its excellent deposition conformal properties, vertical TFT and reduced pixel regions for high resolutions can be realized. The conductivity of thick In_2O_3 film makes it not suitable for electrical gating. Technically, the thickness has been reported to be an important factor to enable gating.[9,11,25] Thick oxide semiconductors have a high carrier density and thus cannot be controlled as a device,

J.-H. Lee, S.-Y. Kang, J.-H. Yang, J.-E. Pi, C.-S. Hwang, J. Moon
Reality Devices Research Division
Electronics and Telecommunication Research Institute (ETRI)
Daejeon 34129, Republic of Korea
E-mail: jmoon@etri.re.kr

J.-H. Lee, J. Moon
Advanced Device Technology
ICT
University of Science and Technology (UST)
Daejeon 34113, Republic of Korea

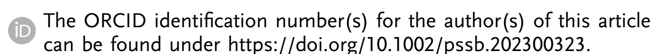
The ORCID identification number(s) for the author(s) of this article can be found under https://doi.org/10.1002/pssb.202300323.

© 2023 The Authors. physica status solidi (b) basic solid state physics published by Wiley-VCH GmbH. This is an open access article under the terms of the Creative Commons Attribution-NonCommercial-NoDerivs License, which permits use and distribution in any medium, provided the original work is properly cited, the use is non-commercial and no modifications or adaptations are made.

DOI: 10.1002/pssb.202300323

15213951, 2024, 7, Downloaded from https://onlinelibrary.wiley.com/doi/10.1002/pssb.202300323 by Electronics and Telecommunications, Wiley Online Library on [11/07/2024]. See the Terms and Conditions (https://onlinelibrary.wiley.com/terms-and-conditions) on Wiley Online Library for rules of use; OA articles are governed by the applicable Creative Commons License

whereas thin oxide semiconductors with a low carrier density are feasible with devices due to the control of the electrical properties. Modern integrated circuit technology requires improved functionality and high performance through scaled channel lengths (L_{ch}) as well as an ultrathin body.[26,27] In particular, the electrical properties and structural characteristics of semiconductor materials depend on the film thickness, and when applied to devices, they are not necessarily predictable.[28–32] Typically, when L_{ch} changes, the mobility changes, which is very important from a scaling perspective. Regarding this scaling issue, we fabricated TFTs with ultrathin In_2O_3 film and a channel thickness of 5 nm. We used an ALD method to deposit ultrathin In_2O_3 films. Most quaternary- (e.g., a-IGZO) and ternary- (e.g., a-IZO) oxide channel materials were investigated as functions of the thickness, contact resistance (R_c), or L_{ch} variation size.[10,13,17–20,22–25,33–36] Although many studies have investigated methods by which to control the high mobility and conductivity of In_2O_3 as a channel material,[9,26] quantitative studies of the R_c and L_{ch} effects present in ultrathin binary oxide channel TFTs are insufficient. Herein, we fabricated ultrathin (5 nm) In_2O_3 film transistors (ultrathin In_2O_3 TFTs) using ALD. To determine the dependence of μ_{FE} on L_{ch}, TFTs with L_{ch} values from 5 to 160 μm at a fixed width of 20 μm were investigated. To ascertain the dependence, we used the transmission line model (TLM)[26,34,37] and extracted R_C, the channel resistivity (ρ), and the total resistance (R_{total}) from the output characteristics under $V_{GS} = 1$, 3, and 5 V. Our study demonstrates a strategic approach for the commercial application of the impact of R_c as downscaled TFTs with reduced ultrathin body channels.

2. Results and Discussion

In_2O_3 can exhibit high field mobility in an amorphous state, showing high conductivity due to the existing trap-neutral level above the CBM.[9] Given that oxygen vacancies (V_O) serve as donors in In_2O_3 film, it is necessary to lower the V_O concentration to enable electrical gating. In this work, we utilized annealing in an O_2 atmosphere for 2 h at 300 °C to lower the V_O concentration. As indicated by the X-ray diffraction three peaks in **Figure 1**a, the ultrathin In_2O_3 film is crystalline. Interplanar spacings of 0.29, 0.17, and 0.15 nm correspond to the (222), (440), (622) planes of cubic bixbyite In_2O_3 (ICDD Card No. 01-0733-6440). Also, the morphology of the crystallized In_2O_3 film was observed by a TEM, as shown in Figure 1b. The TEM bright-field image shows a clear lattice fringe, which corresponds to the (222) plane. From the structural analysis, we conclude that our ALD processing and annealing conditions yield a fully crystallized In_2O_3 film with a bixbyite structure on the ALD-Al_2O_3 gate dielectric layer.

Figure 2a–f shows the transfer characteristics of our In_2O_3 TFT as a function of L_{ch}. In this study, the gate voltage (V_{GS}) ranges from −15 to 20 V and the drain voltage (V_{DS}) varies as 0.1 and 1.0 V. The off-state current and gate leakage current (I_G) levels were lower than 10^{-13} A. The low I_G is mainly due to the excellent gate insulator of Al_2O_3. The drain current (I_D) on/off ratio is approximately 10^7 for all channel sizes. The maximum I_D values in the accumulation regime were observed to decrease as L_{ch} increased, indicating device parameter dependency on L_{ch}. The decrease in the maximum I_D values is thought to have its origin in R_{total}, which is proportional to L_{ch} for a given W. That is, it is likely that I_D of the TFT is affected by other factors in addition to μ. For the general μ_{FE} case, this represents a measure that shows how well the carrier transfer is horizontally transported when V_{GS} is applied. However, this does not mean that pure semiconductor resistivity is independent of other external factors.

We extracted μ_{FE} and plotted it, as shown in **Figure 3**, for a more in-depth assessment. Figure 3 shows the average μ_{FE} value of the eight TFT samples as L_{ch} is varied. In general, while numerous studies of bulk binary metal oxides have been done,[13,34,35] ultrathin binary oxides as a channel component have only recently attracted technical interest.[33,37] Presumably due to the difficulties associated with forming and patterning ultrathin binary oxides as a device component in a stable manner, quantitative reports of μ_{FE} variations in fully fabricated devices are rather scarce. Regarding this issue, we investigated the dependence of μ_{FE} on L_{ch}. We pay close attention to the role of R_c by means of TLM. As is apparent in Figure 3, μ_{FE} increases gradually as L_{ch} increases. Our In_2O_3 TFT exhibited high mobility (35.4 $cm^2\,V^{-1}\,s^{-1}$) comparable to those in a previous study.[22]

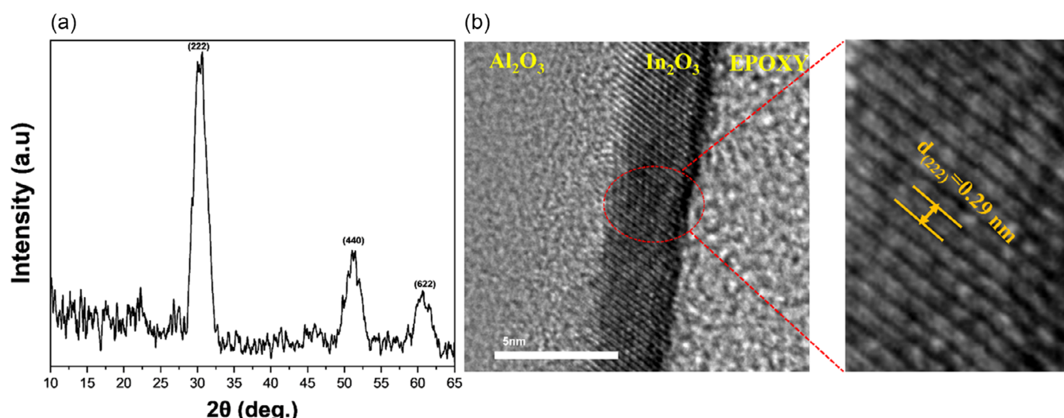

Figure 1. a) The X-ray diffraction (XRD) patterns using Cu-Kα radiation of the crystalline In_2O_3 thin film with 5 nm channel thickness shows the three peaks. b) (Left) cs-corrected scanning transmission electron microscope (cs-TEM) image of the ultrathin In_2O_3 film having a 5 nm thickness structure. (Right) The lattice fringe shows the lattice spacing of 0.29 nm corresponding (222) plan of the cubic bixbyite (ICDD card No. 01-073-6440).

© 2023 The Authors. physica status solidi (b) basic solid state physics published by Wiley-VCH GmbH

15213951, 2024, 7, Downloaded from https://onlinelibrary.wiley.com/doi/10.1002/pssb.202300323 by Electronics and Telecommunications, Wiley Online Library on [11/07/2024]. See the Terms and Conditions (https://onlinelibrary.wiley.com/terms-and-conditions) on Wiley Online Library for rules of use; OA articles are governed by the applicable Creative Commons License

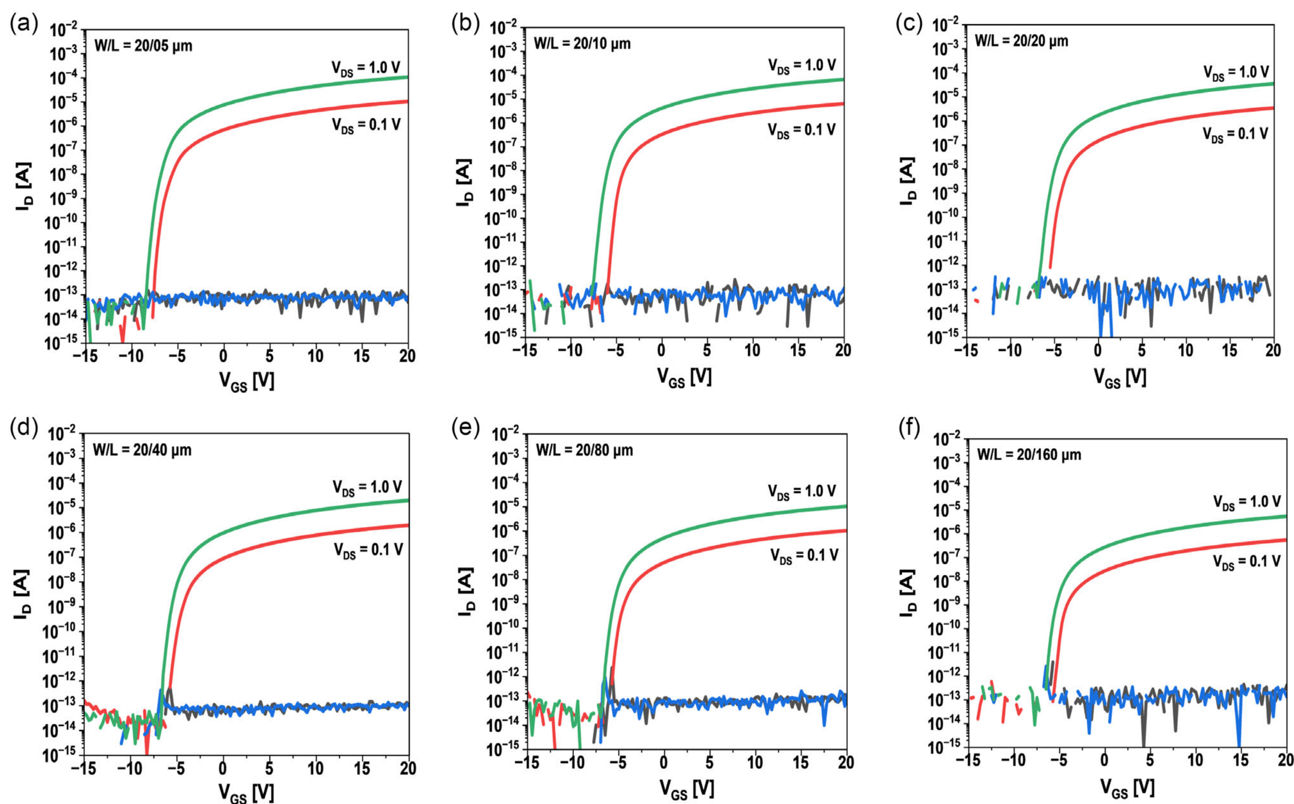

Figure 2. The transfer characteristics of 5 nm In_2O_3 film transistors ranging from −15 to 20 V at $V_{DS} = 0.1$, and 1.0 V, respectively, for a–f) different channel length.

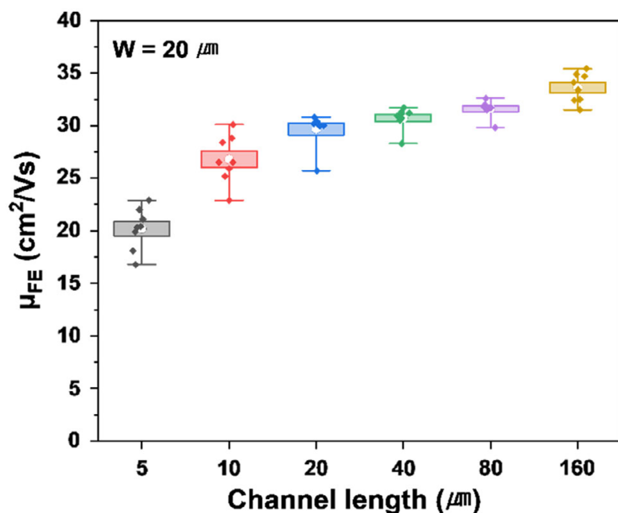

Figure 3. This plot presents the field-effect mobility dependence on the channel length of 8 samples for each channel length. The average μ_{FE} 20.2 $cm^2 V^{-1} s^{-1}$ at $L_{ch} = 5$ μm, 33.6 $cm^2 V^{-1} s^{-1}$ at $L_{ch} = 160$ μm.

Our results indicate the technical possibility of fabricating reliable devices with fairly high mobility levels without the need to resort to ternary or quaternary types of complex oxides. In general, pure semiconductor resistance is described as $\rho = (nq\mu)^{-1}$, where n is the carrier density, q is the electric charge, and μ is the mobility. ρ denotes the specific resistivity, which is a resistance value that does not change as a parameter representing the intrinsic resistance value of the material. Therefore, the aforementioned formula implies that pure semiconductors have a constant μ. However, as shown in Figure 3, it was observed that μ changes as L_{ch} changes. The measurement results indicate additional factors, in addition, contribute to μ.[9,13,33–35,37] According to previous reports, in devices, R_{total} is reported to be the semiconductor's own ρ and R_c arising from the contact between the semiconductor (In_2O_3) and the source/drain (ITO) electrode.

We used the TLM method for quantitative analysis of R_c of an ultrathin binary semiconductor with changes of L_{ch}. For the quantitative analysis of the In_2O_3 TFT, L_{ch} is expressed as a variable, as shown in **Figure 4**. In order to apply the TLM method mentioned earlier, the linear region (ohmic region) of the output characteristics is set in the range of 0–0.5 V, and the end of the output curve starts at the origin. The output characteristics were measured in the V_{GS} range of 1–5 V at 2 V intervals. I_D increases as V_{GS} increases and L_{ch} becomes shorter. Here, n-type TFT output behavior is clearly observed as the V_{GS} polarity and magnitude change.

Figure 5a shows the plotted resistance of all L_{ch} outcomes to obtain the In_2O_3 TFT's R_c value, and Figure 5b presents the ratio of the R_c variable considering L_{ch}. R_{total} from the TLM

© 2023 The Authors. physica status solidi (b) basic solid state physics published by Wiley-VCH GmbH

15213951, 2024, 7, Downloaded from https://onlinelibrary.wiley.com/doi/10.1002/pssb.202300323 by Electronics and Telecommunications, Wiley Online Library on [11/07/2024]. See the Terms and Conditions (https://onlinelibrary.wiley.com/terms-and-conditions) on Wiley Online Library for rules of use; OA articles are governed by the applicable Creative Commons License

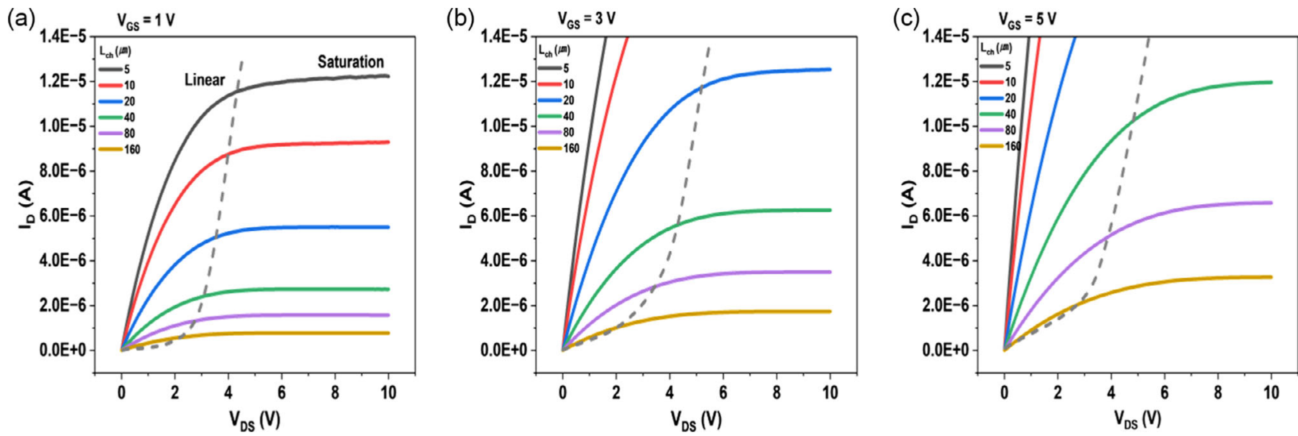

Figure 4. The output characteristics of 5 nm-In_2O_3 TFT ranging from $V_{DS} = 0$ to 10 V at a–c) V_{GS} in the range of 1–5 V.

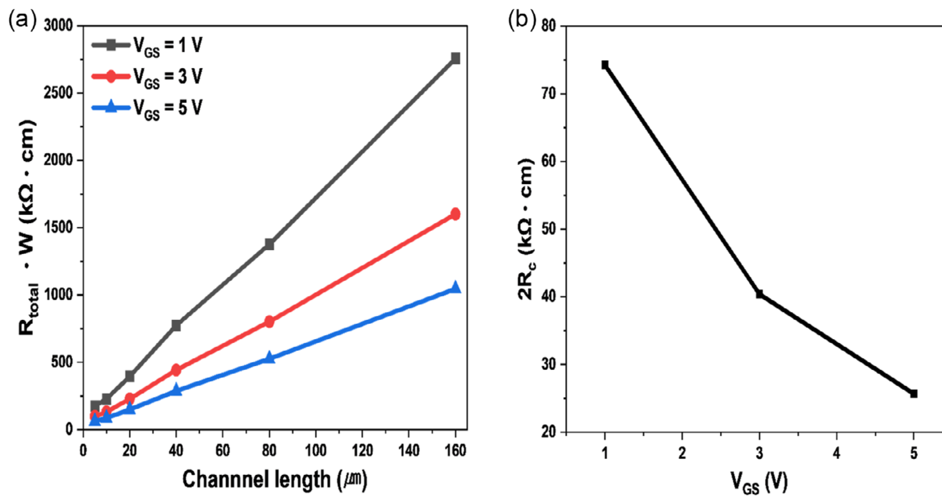

Figure 5. Extracted from the output characteristics of In_2O_3 film transistors at a fixed width of 20 μm by TLM: a) (R_{total} • W) exhibiting the channel resistivity (ρ) as the slope of all ultrathin In_2O_3 film TFTs in this study. b) In_2O_3 $2R_c$ (kΩ cm) behavior from operating In_2O_3 TFTs.

quantitative analysis is expressed as $R_{total} \cdot W = (2R_c \cdot W) + (R_s \cdot L)$, or the sum of R_c and the sheet resistance (R_s). Therefore, the TLM method allows the extraction of R_c and R_s for each L_{ch}. R_c is the resistance existing at the metallization/channel interface, which is ITO/In_2O_3 in this study. The y-axis intercept ($2R_c \cdot W$) yields R, while ρ is extracted at 3.34×10^2 Ω cm from the slope of the linear plot of V_{GS} at 1 V, which is found to be identical for all L_{ch}. As the R_s contribution to R_{total} remains invariant, R_c emerges as a dominant factor determining μ, which is proportional to $1/R_{total}$. The In_2O_3 TFT in this study has an $Rc \cdot W$ values from 37 to 13 kΩ cm in V_{GS} from 1 to 5 V at 2 V step increase. We calculated $2Rc/R_{total}$ as a function of V_{GS} to determine the effects of R_c more clearly due to the variation of L_{ch}. The appearance of factor "2" in $2R_c$ is due to the presence of the source and drain. Our device exhibits the increases of $2R_{c/}R_{total}$ as L_{ch} becomes shorter. At $V_{GS} = 1$ V, $2R_{c/}R_{total}$ at $L_{ch} = 5$ μm is 42.33%, whereas $L_{ch} = 160$ μm shows an outcome of only 2.68%, much higher by about 21 times. This L_{ch} dependent $2R_{c/}R_{total}$ persisted and the ratio changed only marginally, regardless of V_{GS}.[38] As a result, as L_{ch} becomes shorter, R_{total} decreases, and due to this, the ratio of R_c increases, resulting in lower In_2O_3 TFT μ_{FE} characteristics. This explains why L_{ch} has a dominant effect on the In_2O_3 TFT mobility characteristics in addition to R_{total}. Therefore, although the binary oxide (In_2O_3) has a high μ_{FE}, it has been observed that L_{ch} decreases and μ_{FE} decreases due to a high $2R_c$ ratio. As a result, the oxide semiconductor material exhibits lower original characteristics during the TFT deposition process.

As shown by the table in **Figure 6**, the V_{DS} shows the lowest value when $V_{GS} = 1$ V is applied at a $L_{ch} = 5$ μm. We presumed that the V_{DS} is not applied sufficiently to the devices due to the highest R_c ratio. To obtain the correct μ_{FE}, we used the simple conventional equation followed $R_{total} = R_c + R_{ch}$ by applying the corrected $V_{DS}{'}$. As a result, we obtained a consistent μ_{FE} about 34 $cm^2 V^{-1} s^{-1}$ regardless of L_{ch}. However, in the case of the short L_{ch}, it shows slightly lower about 31 $cm^2 V^{-1} s^{-1}$ than other L_{ch} due to the highest R_c ratio in this study. We also assume that when the indium-based film is simultaneously used in the source/drain, the active layer may be affected by the post-annealing in an oxygen atmosphere. As can be seen from previously reported literature

© 2023 The Authors. physica status solidi (b) basic solid state physics published by Wiley-VCH GmbH

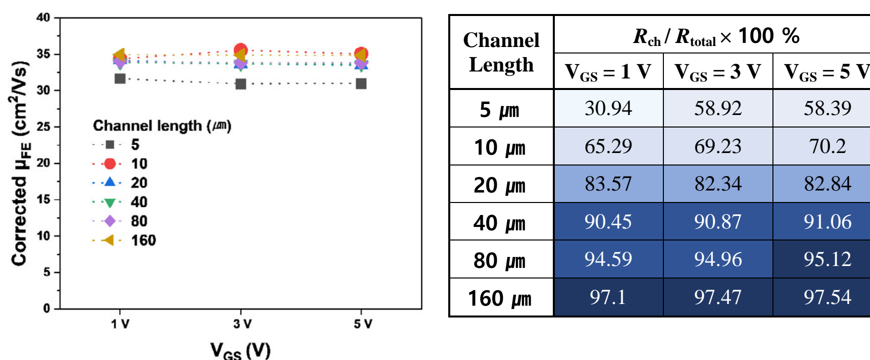

Channel Length	$R_{ch}/R_{total} \times 100$ %		
	$V_{GS} = 1$ V	$V_{GS} = 3$ V	$V_{GS} = 5$ V
5 μm	30.94	58.92	58.39
10 μm	65.29	69.23	70.2
20 μm	83.57	82.34	82.84
40 μm	90.45	90.87	91.06
80 μm	94.59	94.96	95.12
160 μm	97.1	97.47	97.54

Figure 6. The table on the right shows the V_{DS} ratio across the practical devices. The left shows the In_2O_3 TFT μ_{FE} by applying a modified V_{DS}'.

related to this,[9,20,21,25,33] the In_2O_3 film has a nature of high conductivity because of the high carrier density such as an oxygen vacancy (V_o) in film. As shown by the Lee group[21] report, compared to a varied annealing atmosphere such as in air or vacuum, the nano-crystalline In_2O_3 film showed stable semiconductor's electrical properties in an oxygen annealing atmosphere. This was accomplished by making the In_2O_3 layer thickness–5 nm–by using ALD while also annealing in the oxygen atmosphere to add oxygen atoms to the oxygen defects. In the other word, this is due to the bixbyite-based materials' unusual crystal-defect structure, which allows for simple assimilation of oxygen at the surface.[39] According to the facts, oxygen vacancies serving as donors are reduced and resistance is increased at the same time by filling oxygen atoms in the oxygen vacancies existing inside the film due to the post-annealing in an oxygen atmosphere thereby increasing R_c between the electrode and the active layer.

3. Conclusion

In conclusion, in this paper, an ultrathin (5 nm) In_2O_3 TFT device was fabricated through ALD and factors influencing the mobility as it pertains to L_{ch} were quantitatively analyzed through the TLM method. The TLM analyses strongly imply that the R_c fraction occupies a large fraction in R_{total} as L_{ch} decreases. Thus, the TFT mobility decreases as L_{ch} decreases, primarily due to the influence of R_c. This implies that for a given oxide channel material, the electrical contact between the semiconductor and the source/drain electrodes affects the TFT mobility considerably. This might be due to the incorporation of oxygen during the oxygen atmosphere heat treatment of In_2O_3, which lowers the carrier concentration of the ITO/In_2O_3 interface. In summary, we quantitatively show that the main influence on the TFT is R_c rather than the properties of the semiconductor material itself as L_{ch} becomes shorter. This suggests that the relationship between L_{ch} and the semiconductor contact is an important factor when oxide TFT scaling is considered.

4. Experimental Section

Our ultrathin In_2O_3 film transistor [S1] was fabricated as follows: To prepare a non-alkaline glass substrate, the substrate was thoroughly cleaned using an ultrasonic sonicator with acetone, isopropyl alcohol, and DI water. First, a 100 nm Mo gate electrode was formed using DC magnetron sputtering. A 100 nm gate insulator of ALD-Al_2O_3, which was formed using trimethyl-aluminum and H_2O vapor as Al and O precursors, was deposited at 150 °C. A 150 nm ITO thick, which is a Sn-doped indium oxide, was formed to serve as the source/drain electrodes. An In_2O_3 thin film to ensure an ultrathin thickness ($\leq$5 nm), which acts as an active layer, was deposited at 300 °C by means of ALD (Lucida D100, NCD). The In_2O_3 thin film was deposited by combining (3-(dimethylamino)propyl)dimethylindium, DADI) and O_3 (ozone) at 300 °C. DADI is a metal precursor and is delivered into the reaction chamber at a high purity (99.9%) level at a flow rate of 70 cm^3 min^{-1}. A single cycle consists of the following sequential process: In precursor (0.5 s)- Ar purge (10 s)- Ozone (0.2 s)- Ar purge (10 s). This process was repeated until the desired thickness (5 nm) was achieved. The indium oxide deposition growth rate was 1.02 nm $cycle^{-1}$ at 300 °C. The active layer was then patterned via photolithography and wet etching; this was followed by annealing at 300 °C for 2 h in an oxygen atmosphere. The electrical characteristics of the In_2O_3 TFT were measured using a parameter analyzer (Agilent 4155C) in a dark state. The thin film's crystallinity and the structure of the indium oxide as a channel layer were characterized by a high-resolution thin-film X-ray diffractometer (X'Pert-PRO MRD, PANalytical) and by transmission electron microscopy (TEM, JEM-ARM200F, JEOL), respectively.

Supporting Information

Supporting Information is available from the Wiley Online Library or from the author.

Acknowledgements

This work was supported by the National Research Foundation of Korea (NRF) grant funded by the Korea government (MSIT) (NRF-2020M3H4A3081897).

Conflict of Interest

The authors declare no conflict of interest.

Data Availability Statement

The data that support the findings of this study are available from the corresponding author upon reasonable request.

© 2023 The Authors. physica status solidi (b) basic solid state physics published by Wiley-VCH GmbH

15213951, 2024, 7, Downloaded from https://onlinelibrary.wiley.com/doi/10.1002/pssb.202300323 by Electronics and Telecommunications, Wiley Online Library on [11/07/2024]. See the Terms and Conditions (https://onlinelibrary.wiley.com/terms-and-conditions) on Wiley Online Library for rules of use; OA articles are governed by the applicable Creative Commons License

Keywords

atomic layer deposition, contact resistance, indium oxide, n-type oxide semiconductors, scaled channel length, transmission line model

Received: July 20, 2023
Revised: October 30, 2023
Published online: November 3, 2023

[1] E. Fortunato, P. Barquinha, R. Martins, *Adv. Mater.* **2012**, *24*, 2945.
[2] J. F. Wager, R. Hoffman, *IEEE Spectrum* **2011**, *48*, 42.
[3] K. Nomura, H. Ohta, A. Takagi, T. Kamiya, M. Hirano, H. Hosono, *Nature* **2004**, *432*, 488.
[4] X. Yu, T. J. Marks, A. Facchetti, *Nat. Mater.* **2016**, *15*, 383.
[5] A. Liu, G. X. Liu, H. H. Zhu, F. Xu, E. Fortunato, R. Martins, F. K. Shan, *ACS Appl. Mater. Interfaces* **2014**, *6*, 17364.
[6] C. Zhu, A. Liu, G. Liu, G. Jiang, Y. Meng, E. Fortunato, R. Martins, F. Shan, *J. Mater. Chem. C* **2016**, *4*, 10715.
[7] K. Nomura, A. Takagi, T. Kamiya, H. Ohta, M. Hirano, H. Hosono, *Jpn. J. Appl. Phys.* **2006**, *45*, 4303.
[8] T. Kamiya, H. Hosono, *NPG Asia Mater.* **2010**, *2*, 15.
[9] M. Si, Y. Hu, Z. Lin, X. Sun, A. Charnas, D. Zheng, X. Lyu, H. Wang, K. Cho, P. D. Ye, *Nano Lett.* **2021**, *21*, 500.
[10] R. L. Weiher, R. P. Ley, *J. Appl. Phys.* **1966**, *37*, 299.
[11] K. Nomura, H. Ohta, K. Ueda, T. Kamiya, M. Hirano, H. Hosono, *Science* **2003**, *300*, 1269.
[12] H. Hosono, *Thin Solid Films* **2007**, *515*, 6000.
[13] S. Samanta, K. Han, C. Sun, C. Wang, A. V. Y. Thean, X. Gong, in *2020 IEEE Symp. on VLSI Technology*, IEEE, Piscataway, NJ June **2020**, pp. 1–2.
[14] H. Hosono, N. Kikuchi, N. Ueda, H. Kawazoe, *J. Non-Cryst. Solids* **1996**, *198*, 165.
[15] J. Robertson, S. J. Clark, *Phys. Rev. B* **2011**, *83*, 075205.
[16] P. D. C. King, T. D. Veal, D. J. Payne, A. Bourlange, R. G. Egdell, C. F. McConville, *Phys. Rev. Lett.* **2008**, *101*, 2.
[17] A. M. Ganose, D. O. Scanlon, *J. Mater. Chem. C* **2016**, *4*, 1467.
[18] T. De Boer, M. F. Bekheet, A. Gurlo, R. Riedel, A. Moewes, *Phys. Rev. B* **2016**, *93*, 155205.
[19] W. Hu, R. L. Peterson, *Appl. Phys. Lett.* **2014**, *104*, 192105.
[20] J. Moon, J. M. Lee, H. J. Lee, J. E. Pi, J. Na, S. D. Ahn, S. Y. Kang, *Phys. Status Solidi A* **2021**, *218*, 2000750.
[21] J. Lee, J. Moon, J. E. Pi, S. D. Ahn, H. Oh, S. Y. Kang, K. H. Kwon, *Appl. Phys. Lett.* **2018**, *113*, 112102.
[22] H. I. Yeom, J. B. Ko, G. Mun, S. H. K. Park, *J. Mater. Chem. C* **2016**, *4*, 6873.
[23] J. S. Ponraj, G. Attolini, M. Bosi, *Crit. Rev. Solid State Mater. Sci.* **2013**, *38*, 203.
[24] S. M. George, *Chem. Rev.* **2010**, *110*, 111.
[25] Z. Qiao, R. Latz, D. Mergel, *Thin Solid Films* **2004**, *466*, 250.
[26] C. P. T. Nguyen, T. T. Trinh, J. Raja, A. H. T. Le, Y. J. Lee, V. A. Dao, J. Yi, *Mater. Sci. Semicond. Process.* **2015**, *39*, 649.
[27] G. Li, D. Xie, T. Feng, J. Xu, X. Zhang, T. Ren, *Solid-State Electron.* **2014**, *95*, 32.
[28] S. Lany, A. Zakutayev, T. O. Mason, J. F. Wager, K. R. Poeppelmeier, J. D. Perkins, J. J. Berry, D. S. Ginley, A. Zunger, *Phys. Rev. Lett.* **2012**, *108*, 016802.
[29] T. Koida, Y. Ueno, H. Shibata, *Phys. Status Solidi A* **2018**, *215*, 1700506.
[30] Y. Magari, T. Kataoka, W. Yeh, M. Furuta, *Nat. Commun.* **2022**, *13*, 1078.
[31] P. Mittal, Y. S. Negi, R. K. Singh, *J. Semicond.* **2014**, *35*, 124002.
[32] B. Li, C. Y. Han, P. T. Lai, W. M. Tang, *Thin Solid Films* **2018**, *667*, 28.
[33] M. Si, Z. Lin, Z. Chen, X. Sun, H. Wang, P. D. Ye, *Nat. Electron.* **2022**, *5*, 164.
[34] S. Lee, H. Park, D. C. Paine, *J. Appl. Phys.* **2011**, *109*, 063702.
[35] J. Jeong, G. J. Lee, J. Kim, B. Choi, *J. Phys. D: Appl. Phys.* **2012**, *45*, 135103.
[36] P. Barquinha, A. Vila, G. Gonçalves, L. Pereira, R. Martins, J. Morante, E. Fortunato, *Phys. Status Solidi A* **2008**, *205*, 1905.
[37] S. Lee, Y. Song, H. Park, A. Zaslavsky, D. C. Paine, *Solid-State Electron.* **2017**, *135*, 94.
[38] M. J. Kim, H. J. Park, S. Yoo, M. H. Cho, J. K. Jeong, *IEEE Trans. Electron Devices* **2022**, *69*, 2409.
[39] S. P. Harvey, T. O. Mason, Y. Gassenbauer, R. Schafranek, A. Klein, *J. Phys. D: Appl. Phys.* **2006**, *39*, 3959.

© 2023 The Authors. physica status solidi (b) basic solid state physics published by Wiley-VCH GmbH

15213951, 2024, 7, Downloaded from https://onlinelibrary.wiley.com/doi/10.1002/pssb.202300323 by Electronics and Telecommunications, Wiley Online Library on [11/07/2024]. See the Terms and Conditions (https://onlinelibrary.wiley.com/terms-and-conditions) on Wiley Online Library for rules of use; OA articles are governed by the applicable Creative Commons License